

Preparation of poly(vinyl formal) foams modified by corn stalk fiber and its application in sewage treatment

An Li, Wenling Yang*, Fangcha Wang, Pengrui Zhang, Hulin Li, Boyang Di

Chemical and Pharmaceutical Engineering of Hebei University of Science & Technology, Shijiazhuang, Hebei 050018, China, emails: 1132482882@qq.com (W. Yang), 1846732093@qq.com (A. Li), h18438578039@163.com (F. Wang), 2689560592@qq.com (P. Zhang), 2208952654@qq.com (H. Li), 582351968@qq.com (B. Di)

Received 4 December 2021; Accepted 30 March 2022

ABSTRACT

Novel suspended biocarrier polyvinyl formal foam materials (CSF-PVFM) are prepared through the chemical cross-linking of polyvinyl alcohol and crude corn stalk fiber (CSF). Using Fourier-transform infrared spectroscopy and X-ray diffraction, we confirmed that a chemical cross-linking reaction occurs. Using scanning electron microscopy, we found that the material performs well with an interconnected pore structure, a macroscopically rough surface, and a wide range of pore diameters. Compared with pure PVFM, the addition of CSF results in different degrees of improvement in specific surface area, tensile strength and thermal stability. Orthogonal experiments were carried out to optimize the raw material ratios and the conditions of the preparation technology by adopting porosity, water absorption rates, and specific gravity as the performance evaluation indices, and the CSF-PVFM with the best performance was obtained. Under the best conditions, the average porosity could reach 97.2%, the specific gravity could reach 1.00 g cm⁻³, water absorption could reach 22.58, and the cross-linking degree could reach 96.08%. A further study of sewage treatment using CSF-PVFM as a suspended biocarrier produced good results: the average removal rate of chemical oxygen demand was 93.26%, and the average removal rate of ammonia nitrogen was 96.77%.

Keywords: Polyvinyl formal; Corn stalk crude fiber; Orthogonal experiment; Sewage treatment; Suspended biocarrier

1. Introduction

Major sources of water contamination included the un-regulated discharge of sewage and municipal wastewater, industrial wastewater, and agricultural fertilizers and pesticides. The pollutants in sewage are mainly organic matter, ferrous salt, sulfide, nitrogen, phosphorus, etc. Most of these pollutants are both toxic and inhibitory, and can accumulate through the food chain [1]. These pollutants often have long-term impacts, so they pose a great threat to human health and the survival of animals and plants [2]. Additionally, in recent decades, the tightening of standards

for the discharge of pollutants has indicated that the demand for wastewater treatment processes has strengthened. A broad range of techniques have been applied to sewage treatment, including activated sludge treatment [3], electrodialysis [4], electrocoagulation [5], membrane filtration [6], adsorption [7], chemical oxidation [8], etc. However, each of these methods has some disadvantages, including the production of high volumes of sludge, high operating and maintenance costs, a requirement for large quantities of adsorbents and chemical additives, and the creation of secondary pollution. Accordingly, inexpensive, efficient, and sustainable methods are required to remove

* Corresponding author.

pollutants from sewage [9,10]. Biological treatment methods stand out among those available methods because of their low cost, high efficiency, safety, minimal sludge production and environmental compatibility. The biological treatment processes that have been developed and applied to sewage include biological filtering [11], rotating biological contactors [12], biological contact oxidation [13], etc. In addition, researchers have found a more efficient and superior method. A moving biological bed reactor (MBBR) has the advantages of a traditional biological fluidized bed and the biological contact oxidation process, and has become one of the most efficient and environmentally friendly biological treatment methods in recent years [14]. More importantly, the effectiveness of the MBBR process depends largely on the performance of the suspended biocarrier. Polyurethane [15], polystyrene [16], and polypropylene [17] are ideal suspended biocarriers for sewage treatment. However, the polystyrene material itself has low mechanical strength and low brittleness, and the polyurethane biocarriers are toxic to microorganisms and usually have high cost. The application of a polyethylene/polypropylene biological carrier in sewage treatment is limited because of its surface hydrophobicity and poor biological affinity. Therefore, the low toxicity, low cost, and better performance of suspended biocarriers have shown more practical significance.

Polyvinyl formal foam (PVFM) material is a product of condensation involving polyvinyl alcohol (PVA) and formaldehyde (HCHO), and is an important type of polymer material. When PVFM is used as a biocarrier, it has the advantages of high porosity, density close to that of water, good water absorption, and biocompatibility. At the same time, it has good chemical and biological stability, will not dissolve harmful substances, and does not cause secondary pollution. It has a certain degree of mechanical strength, and it is not easily broken under hydraulic scouring, so it has a long service life. Thus, PVFM foam material has gradually become a popular research topic for a majority of researchers. It has been proven that modifying PVFM can effectively improve its performance as a suspended biocarrier. There has been many studies on adding activated carbon [18], bamboo charcoal [19], attapulgite [20], and fly ash [21] to modify PVFM. Although activated carbon and bamboo charcoal are the most commonly used modifiers, they present some disadvantages, such as high capital and running costs and weak hydrophilic affinity. On the other hand, attapulgite and fly ash are inexpensive and readily available materials, but their biocompatibility is poor. Natural fiber has thus become one of the main study directions for the development of sewage treatment materials in the future because of its advantages of low price, good bioaffinity, and high porosity.

As a kind of green material, natural fiber composite material has become one of the main development directions of sewage treatment materials in the future because of its low price, non-toxic to organisms, and good mass transfer performance. Natural fibers are mainly composed of cellulose, hemicellulose and lignin. Hemicellulose acts as a link between lignin and cellulose [22]. Hemicellulose and lignin exist in an amorphous state and can be easily removed by caustic soda and some solvents. The remaining

cellulose is a linear macromolecule composed of many D-glucopyranose units linked to each other by β -1,4-glycosidic bond, which has good hydrophilicity and provides the possibility of chemical modification of PVFM [23,24]. Feng [25] modified PVFM with Arabic gum fiber to improve the physical and chemical properties of the material, such as porosity, water absorption, surface roughness and specific surface area. The prepared FN-PVFM can shorten the start-up time, but has poor fluidization in the bioreactor.

At present, the modification of PVFM with corn stalk fiber (CSF) is seldom reported and corn straw fiber is a huge resource in the world [26]. The reasonable development and utilization of corn stalks not only helps alleviate the pressures of resource shortages, but also plays a positive role in promoting environmental protection. Therefore, in this study, CSF was innovatively used as the active material to modify PVFM, to prepare a novel environmentally friendly suspended biocarrier, CSF-PVFM. The specific objectives of this work were (a) to obtain the optimal reaction conditions for the preparation of the CSF-PVFM through single-factor experiments and orthogonal experiments, (b) to study the characteristics of the CSF-PVFM with Fourier-transform infrared spectroscopy (FTIR), scanning electron microscopy (SEM), automatic specific surface area analyzer, X-ray diffraction (XRD), and thermogravimetric analyzer (TGA), and (c) to evaluate the ability of the CSF-PVFM to remove chemical oxygen demand (COD) and ammonia nitrogen from sewage.

2. Experimental

2.1. Materials

The corn stalks used as raw material in this study were obtained from a village in Shi Jiazhuang. The corn stalks were sufficiently washed with deionized water and then dried in an oven (101-1A, Tester-Tianjin) at 110°C for 24 h. The dried samples were crushed and sieved to particle sizes in the range of 0.5–1 mm. Sodium hydroxide (NaOH) for the alkali treatment of corn stalks was purchased from the Tianjin Yongda Chemical Reagent Co., Ltd., China. PVA 17–99 (H) was purchased from the Anhui Wanwei High-tech New Materials Co., Ltd., China. HCHO was purchased from the Tianjin Baishi Chemical Co., Ltd., China. Concentrated sulfuric acid (H_2SO_4) was purchased from the Kaifeng Fangjing Chemical Reagent Co., Ltd., China. Sodium dodecyl sulfate (SDS) was purchased from the Tianjin Guangfu Fine Chemical Research Institute, China. Sodium bicarbonate ($NaHCO_3$) was purchased from the Beijing Yili Fine Chemicals Co., Ltd., China. All of the reagents used were analytically pure. Analytical grade formaldehyde had a HCHO content of 37%–40%. Concentrated sulfuric acid had a strength greater than 98%.

2.2. Preparation of CSF-PVFM

2.2.1. Preparation of CSF

Corn stalk powder was pretreated with 3% NaOH at 45°C for 1.5 h. Then, 5 g of corn stalk powder was mixed with 100 mL of NaOH in a round-bottomed flask. The

mixture was stirred at a speed of 500 rpm for 1.5 h at 45°C using a precision-enhanced electric mixer (JJ-1100W, Honghua, China). It was afterwards suction-filtered and dried at 50°C to a constant mass to obtain the CSF rich in cellulose and lignin.

2.2.2. Preparation of CSF-PVFM

PVA-mixed deionized water was heated uniformly to 95°C in a water bath to prepare the PVA solution and then cooled to room temperature for use. First, the PVA solution, CSF, and SDS were added together in a stoppered three-necked flask and stirred to form a white pre-polymer with a stirring speed of 700 rpm in a water bath maintained at a constant temperature. The catalyst, a concentrated sulfuric acid, was then added to the pre-polymer drop by drop. Next, the cross-linker HCHO was also dripped into the mixture, which was simultaneously stirred at a speed of 300 rpm. Last, the NaHCO₃ blowing agent was added to the mixture with a stirring speed of 700 rpm until the reaction produced the product, which was then poured into a mold and dried for 6 h at 60°C. The molded product was washed and dried overnight at 60°C to obtain the porous material, CSF-PVFM.

2.3. Structural characterization of sample

2.3.1. Fourier-transform infrared spectroscopy

Fourier-transform infrared spectrometer (FT-135, Bio-RAD, US) was used to record the IR spectra of the samples at room temperature. The sample was mixed with potassium bromide and thoroughly ground in agate mortar. The mixture was then transferred to a mold and pressed into transparent sheets.

2.3.2. X-ray diffraction

The X-ray diffractometer (D/MAX-2500, Rigaku) was used to measure XRD spectra. The angle of diffraction was varied from 10° to 35°.

2.3.3. Scanning electron microscopy

The internal structure of the sample was studied using scanning electron microscope (S-4800-I, HITACHI, Japan). The sample was coated with a thin conductive layer of gold.

2.3.4. Automatic specific surface area analyser

The specific surface area of the material was determined using Automatic specific surface area analyzer (NOVA2000, Quantachrome, US). Nitrogen was used as the adsorbate, and the specific surface area of the sample was determined according to Brunauer–Emmett–Teller (BET).

2.4. Characterization of the sample properties

2.4.1. Tensile strength

The tensile strength (R_m) of the material was analysed [27,28].

2.4.2. Porosity

The dry material was cut into small cubes with a volume of 1 cm³. The porosity (ϵ) was calculated by Eq. (1):

$$\epsilon(\%) = \left(1 - \frac{m}{\rho}\right) \times 100 \quad (1)$$

where m (g) is the mass, and ρ (g cm⁻³) is 1.2.

2.4.3. Specific gravity

The dry material was cut into small cubes. The specific gravity (ω) was calculated by Eq. (2):

$$\omega(\text{g/cm}^3) = \frac{M}{V} \quad (2)$$

where V (cm³) is the volume, and M (g) is the mass of the material immersed in distilled water and fully expanded.

2.4.4. Water absorption

The water absorption (A) was calculated by Eq. (3):

$$A = \frac{M - m}{m} \quad (3)$$

where m (g) is the mass, and M (g) is the mass of the material immersed in distilled water and fully expanded.

2.4.5. Cross-linking degree

The cross-linking degree (J) calculated by Eq. (4):

$$J(\%) = \frac{m_1}{m_2} \times 100 \quad (4)$$

where m_1 (g) is the mass and m_2 (g) is m is the mass of the material after putting it in distilled water at 95°C for 24 h.

2.5. Optimize experimental design

2.5.1. Experimental design based on single-factor analysis

Many researchers have found that these parameters (such as the reaction temperature of the system, the amount of each raw material, etc.) have a great influence on the porosity, specific gravity, water absorption, and cross-linking degree of suspended biocarriers. To analyze the effect of a single influencing factor on the experimental result, while not considering the interactions between different factors, a single-factor analysis method was first used in this experiment (Table 1). When the effect of one factor was discussed, the other factors were fixed. Each experiment was repeated three times.

2.5.2. Orthogonal experiments design

According to the results of a previous single-factor experiment, an orthogonal experiment was designed

using online application SPSSAU. As shown in Table 2, the orthogonal experiment was designed according to the $L_{18}(3^7)$ table with six variables: PVA mass concentration (A), CSF dosage (B), H_2SO_4 dosage (C), HCHO dosage (D), $NaHCO_3$ dosage (E), and reaction temperature (F). In addition, the blank group (G) was set-up. The following were the three values of the six variables: A: 9%, 10%, and

11%; B: 0.3, 0.4, and 0.5 g; C and D: 4, 5, and 6 mL; E: 0.58, 0.63, and 0.68 g; and F: 40°C, 45°C and 50°C, respectively (Table 3). Each experiment was repeated three times.

Table 1
Screening of experimental conditions

Factors	Conditions
PVA mass concentration (%)	8, 9, 10, 11, 12
CSF dosage (g)	0.2, 0.3, 0.4, 0.5, 0.6
H_2SO_4 dosage (mL)	4, 5, 6, 7, 8
HCHO dosage (mL)	4, 5, 6, 7, 8
$NaHCO_3$ dosage (g)	0.53, 0.58, 0.63, 0.68, 0.73
Reaction temperature (°C)	35, 40, 45, 50, 55

Table 2
Factors and levels of orthogonal experiment

Treatment	Factors						
	A	B	C	D	E	F	G
1	9	0.3	4	4	0.58	40	1
2	10	0.4	5	5	0.63	45	2
3	11	0.5	6	6	0.68	50	3

A: PVA mass concentration (%); B: CSF dosage (g); C: H_2SO_4 dosage (mL); D: HCHO dosage (mL); E: $NaHCO_3$ dosage (g); F: reaction temperature (°C).

Table 3
Experimental design

Treatment	A (%)	B (g)	C (mL)	D (mL)	E (g)	F (°C)	G
1	9	0.3	4	4	0.58	40	1
2	9	0.4	5	5	0.63	45	2
3	9	0.5	6	6	0.68	50	3
4	10	0.3	4	5	0.63	50	3
5	10	0.4	5	6	0.68	40	1
6	10	0.5	6	4	0.58	45	2
7	11	0.3	5	4	0.68	45	3
8	11	0.4	6	5	0.58	50	1
9	11	0.5	4	6	0.63	40	2
10	9	0.3	6	6	0.63	45	1
11	9	0.4	4	4	0.68	50	2
12	9	0.5	5	5	0.58	40	3
13	10	0.3	5	3	0.58	50	2
14	10	0.4	6	4	0.63	40	3
15	10	0.5	4	5	0.68	45	1
16	11	0.3	6	5	0.68	40	2
17	11	0.4	4	6	0.58	45	3
18	11	0.5	5	4	0.63	50	1

2.6. Experimental design of sewage treatment

To determine the feasibility of CSF-PVFM as a suspended biocarrier, we experimentally studied how it affected the removal of sewage pollutants. We conducted the experiment in three main stages: the start-up period, the improvement period, and the stable period.

- The sewage was obtained from the sewage treatment station of Hebei University of Science and Technology. The concentration of influent COD was 410–890 $mg L^{-1}$, and the concentration of influent ammonia nitrogen was between 75–110 $mg L^{-1}$. The pH of the sewage was adjusted with $NaHCO_3$ to maintain it between 6 and 9 [29].
- The sewage treatment experiment was conducted in a reactor with an effective volume of 4 L at 30°C. The CSF-PVFM was cut into cubes and placed into the reactor until it was at 20% capacity. The experiment adopted a method involving intermittent water inflow and polluted water entered the reactor from the bottom. The reactor was aerated using an air pump (DIKMA-1), which maintained the amount of dissolved oxygen (DO) between 2 and 4 $mg L^{-1}$ [30].
- The CSF-PVFM and sewage were added to the reactor, and the aeration rate was controlled at 3 $L min^{-1}$ to form the biofilm and to remove the pollutants. Samples of raw sewage, effluent water, and deionized water were collected every day. The COD content in the sample

was determined according to the national standard, the “Water Quality Determination of Chemical Oxygen Demand Dichromate Method”, and the ammonia nitrogen content was determined according to the industry standard, the “Water Quality Determination of Ammonia Nitrogen-Nessler’s Reagent Spectrophotometry”. The standard curve of ammonia nitrogen was determined in the experiment (Fig. 1).

3. Results and discussion

3.1. Analysis of the IR spectra

To verify the cross-link reaction, FTIR analysis was used to study the absorption peaks and the corresponding functional groups of PVA and CSF-PVFM (Fig. 2). For PVA, a broad band peaked at $3,422\text{ cm}^{-1}$, corresponding to the $-\text{OH}$; the $-\text{CH}_2$ peak was observed at $2,945\text{ cm}^{-1}$ [31]. For CSF-PVFM, four sharp absorption bands in the range of $1,250\text{--}1,000\text{ cm}^{-1}$ were its characteristic peaks, which were generated by an acetal bond with a structure of 1,3-dioxane [32]. These characteristic absorption peaks were reflected in the infrared spectrum of the CSF-PVFM, indicating that the cross-linking reaction occurred. The characteristic peak of the intensities of the hydroxyl radical group transferred from $3,422$ to $3,455\text{ cm}^{-1}$, indicating that the CSF-PVFM containing $-\text{OH}$ still had strong hydrogen bonds. Therefore, CSF-PVFM used as a suspended filler had good hydrophilicity and excellent biological affinity.

3.2. Analysis of the XRD

The X-ray diffraction patterns of the CSF-PVFM and PVA membranes are given in Fig. 3. As can be seen, the high-intensity diffraction peak at $2\theta = 18.83^\circ$ is the characteristic diffraction peak of PVA. The XRD pattern of CSF-PVFM is similar to that of PVA, but the peak pattern becomes wider, which may be caused by the reaction of PVA with formaldehyde and CSF, the chemical reaction of the $(-\text{OH})$ hydroxyl group in the original structure of PVA, and the weakening of hydrogen bond association [33].

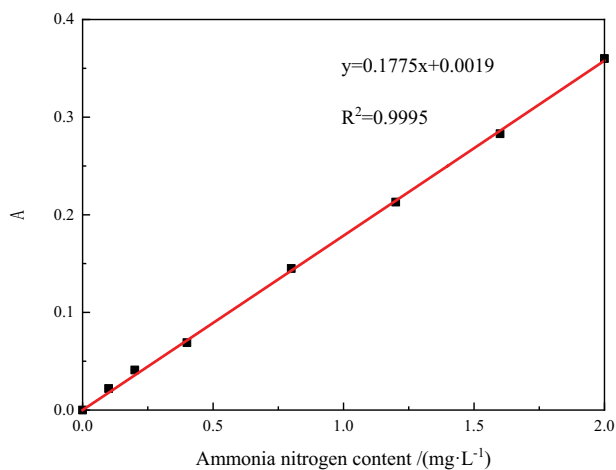


Fig. 1. Standard curve of $\text{NH}_4^+\text{-N}$.

3.3. Analysis of the surface morphology

3.3.1. Analysis of the SEM

Fig. 4 shows the typical SEM images of CSF-PVFM. In agreement with our expectations, the foam morphology adopted a significant three-dimensional network structure when CSF-PVFM foams were prepared in optimal conditions. When the mold was completely filled with the foaming material, the growth of the foam cells was restricted before its natural end, leading to a short growth time for bubbles, which reduced coalescence and the rupturing of bubbles. Thus, a CSF-PVFM with abundant foam cells was obtained. In addition, it was also found that the foam cells have a wide range of pore diameters, which is conducive for various microorganisms to attach and grow.

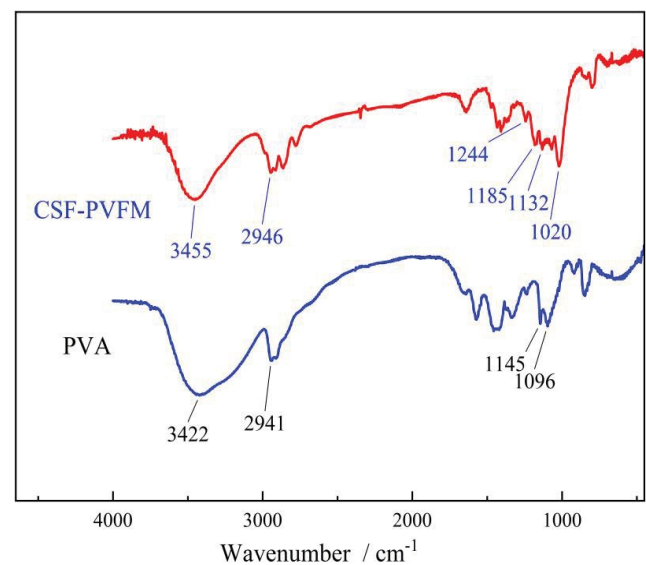


Fig. 2. FTIR spectra of the PVA and CSF-PVFM.

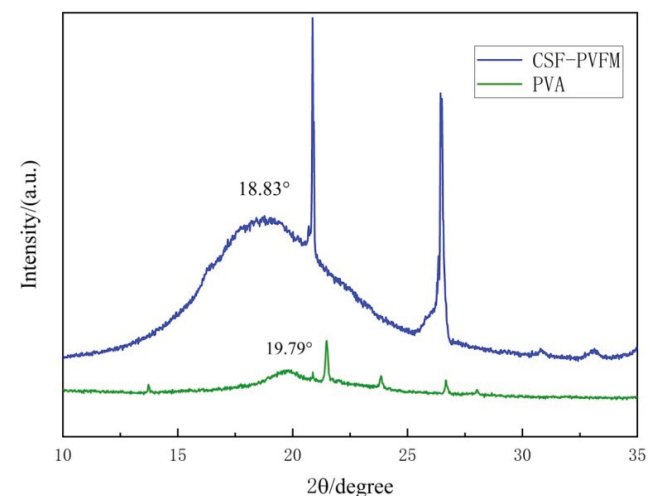


Fig. 3. XRD diffractograms of PVA and CSF-PVFM.

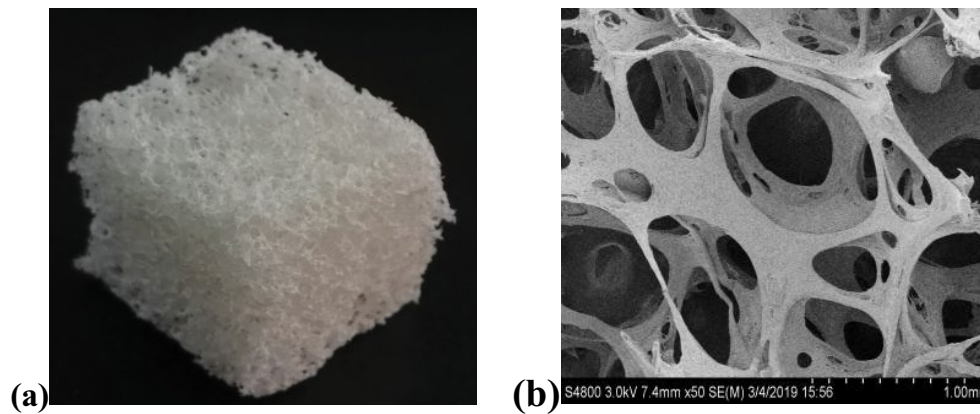


Fig. 4. Morphology and structure of CSF-PVFM: (a) was appearance of CSF-PVFM and (b) was 40× micropore structure of CSF-PVFM.

Table 4
Specific surface area

	PVFM	CSF-PVFM
BET model (single-point method) ($P/P_0 = 0.2$) ($\text{m}^2 \text{g}^{-1}$)	0.9002	1.0572
BET model (multi-point method) ($\text{m}^2 \text{g}^{-1}$)	1.1894	1.5190
Langmuir model ($\text{m}^2 \text{g}^{-1}$)	2.1033	2.7498

Table 5
Tensile strength

Treatment	R_{mPVFM} (MPa)	$R_{mCSF-PVFM}$ (MPa)
1	0.50	0.72
2	0.51	0.76
3	0.55	0.70
Mean	0.53	0.73

3.3.2. Analysis of the specific surface area

The specific surface areas of PVFM and CSF-PVFM measured by the Langmuir model and the BET model are shown in Table 4. The results show that the addition of corn straw fiber inevitably increases the specific surface areas. The specific surface area, according to the BET single-point method, increased from 0.9002 to 1.0572 $\text{m}^2 \text{g}^{-1}$. The specific surface area, according to the BET multi-point method, increased from 1.1894 to 1.5190 $\text{m}^2 \text{g}^{-1}$. The specific surface area of the Langmuir model increased from 2.1033 to 2.7498 $\text{m}^2 \text{g}^{-1}$.

3.4. Analysis of the tensile strength

The CSF had a positive effect on the tensile strength of the foams, as seen in Table 5. Specifically, the tensile strength of CSF-PVFM increased in comparison with that of pure PVFM, and that can be ascribed to an increase in the viscosity of the mixture accompanying the larger fiber content. The result shows that after alkali treatment CSF could improve the mechanical properties of PVFM, and further enabled it to have a certain degree of resistance

to hydraulic erosion when used in sewage treatment, meeting the mechanical requirements of the suspended biocarrier [34].

3.5. Analysis of the optimize experimental results

3.5.1. The single-factor experiment results

The results obtained by single-factor experiment were as follows: a PVA mass concentration of 10%, a CSF dosage of 0.5 g, a H_2SO_4 dosage of 4 mL, a HCHO dosage of 5 mL, a SDS dosage of 0.3 g, a NaHCO_3 dosage of 0.63 g, a reaction temperature of 40°C, a H_2SO_4 dripping time of 6 min, a HCHO dripping time 4 min, and a curing time of 8 h at 60°C.

3.5.2. Orthogonal experiment results

Eighteen experimental groups in the orthogonal experiment were tested to determine the porosity, specific gravity, and water absorption of the CSF-PVFM materials under different material ratios and preparation technology conditions. The results were analysed to determine the best CSF-PVFM material ratio and preparation technology. Table 6 presents the orthogonal table $L_{18}(3^7)$ and the experimental results of each index. This study utilized the range analysis method to treat the results of the orthogonal experiment, and the degree of dispersion of the data was reflected in the data's range and variance.

K_{mj} is the test result corresponding to the level of factor m in column j , and \bar{K}_{mj} is the average value of K_{mj} , $R_j = \max K_{mj} - \min K_{mj}$, Table 7 presents the results. The range determines the degree of significant influence each factor had on the test results.

Table 6
Orthogonal experimental table $L_{18}(3^7)$ and experimental results of each index

	A	B	C	D	E	F	G	ϵ (%)	ω (g cm ⁻³)	A
1	1	1	1	1	1	1	1	96.17	0.87	16.33
2	1	2	2	2	2	2	2	95.67	0.99	21.35
3	1	3	3	3	3	3	3	91.38	0.97	17.56
4	2	1	1	2	2	3	3	97.07	1.08	15.92
5	2	2	2	3	3	1	1	96.79	1.01	19.23
6	2	3	3	1	1	2	2	95.43	1.07	17.21
7	3	1	2	1	3	2	3	96.33	0.98	18.27
8	3	2	3	2	1	3	1	94.76	1.15	15.27
9	3	3	1	3	2	1	2	96.40	1.02	25.58
10	1	1	3	3	2	2	1	94.68	0.95	17.44
11	1	2	1	1	3	3	2	97.04	0.93	18.31
12	1	3	2	2	1	1	3	97.06	1.00	23.89
13	2	1	2	3	1	3	2	92.68	1.06	18.74
14	2	2	3	1	2	1	3	95.82	0.99	19.21
15	2	3	1	2	3	2	1	97.04	1.05	22.45
16	3	1	3	2	3	1	2	95.78	1.04	17.09
17	3	2	1	3	1	2	3	93.50	1.13	20.73
18	3	3	2	1	2	3	1	96.41	1.07	18.63

3.5.3. Analysis of the porosity

Fig. 5 and Table 8 depict the influences of various factors on the porosity of the CSF-PVFM, which follow the order HCHO dosage > H₂SO₄ dosage > reaction temperature > NaHCO₃ dosage > PVA mass concentration > CSF dosage.

PVA is the core material for the synthesis of CSF-PVFM, and the change in its mass fraction had a great influence on the performance of the material. At a PVA mass concentration of 10%, the maximum porosity was reached, and then, the porosity began to decrease with an increase in the PVA mass fraction. With other conditions being maintained as constant, when the PVA mass fraction became too large, the viscosity increased excessively, and the bubbles became wrapped in the liquid film and could not escape smoothly, resulting in low porosity. Therefore, the optimal PVA mass concentration is 10%.

With the increase in the CSF dosage, the porosity increased at first and then tended to remain constant. CSF is also one of the main raw materials for the synthesis of CSF-PVFM. The performance of the material can be improved by using CSF to modify the material. After alkali treatment, the surface roughness of CSF increased, which acted as a nucleating agent. As the amount of CSF increased, the number of bubbles formed also increased, as did the porosity of the biocarrier. The porosity of CSF-PVFM was largest when the CSF content was 0.5 g, and after increasing the amount of CSF, the porosity of CSF-PVFM no longer increased significantly. Therefore, 0.5 g was selected as a reasonable CSF dosage.

The porosity decreased with an increase in the H₂SO₄ dosage. H₂SO₄ was used as a catalyst for the acetalization reaction, and the amount had a great influence not only

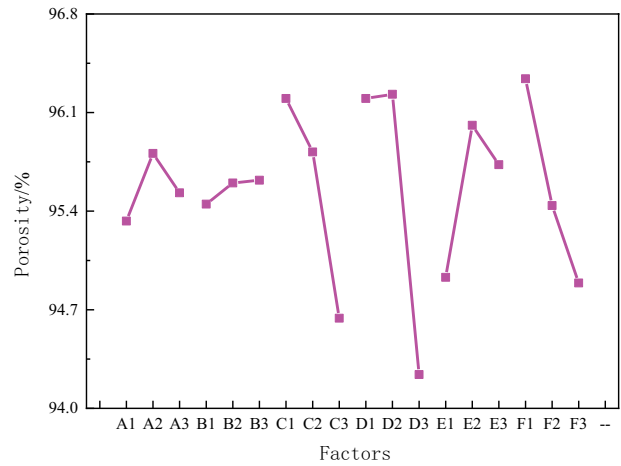


Fig. 5. Tend chart on porosity.

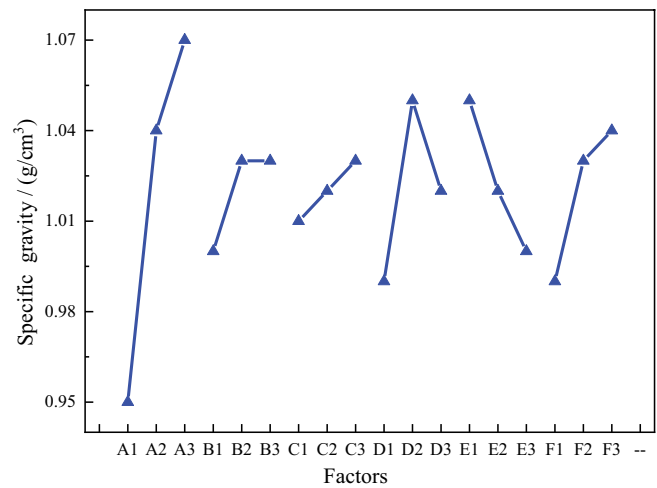


Fig. 6. Tend chart on specific gravity.

on the reaction process but also on the foaming effect of the material. When the amount of H₂SO₄ was more than 4 mL, the porosity dropped rapidly. This occurred because when the sulfuric acid content of the system was too high, the acetal reaction was too fast and the reaction endpoint was difficult to control, which easily causes the raw material to cure in the reactor ahead of its time.

As the HCHO dosage increased, the porosity of the CSF-PVFM first increased and then decreased, showing a normal distribution. As the cross-linking agent and the main raw material for the experiment, the formaldehyde dosage had a great influence on the acetal reaction. If the amount of formaldehyde was too small, it was difficult for the reaction to reach the endpoint, and, at the same time, shaping the raw material became difficult or even impossible in the later stage. When the amount of HCHO was increased to 5 mL, the porosity reached the maximum. When the amount of HCHO increased again, the condensation reaction rate was faster, and a violent condensation reaction occurred, resulting in a large amount of foam becoming deformed or even rupturing, and the porosity decreased.

Table 7
Analysis of orthogonal experimental results

Number		Factors						
		A	B	C	D	E	F	G
ε (%)	K_{1j}	572.00	572.71	577.22	577.20	569.60	578.02	575.85
	K_{2j}	574.83	573.58	574.94	577.38	576.05	572.65	573.00
	K_{3j}	573.18	573.72	567.85	565.43	574.36	569.34	571.16
	\bar{K}_{1j}	95.33	95.45	96.20	96.20	94.93	96.34	95.98
	\bar{K}_{2j}	95.81	95.60	95.82	96.23	96.01	95.44	95.50
	\bar{K}_{3j}	95.53	95.62	94.64	94.24	95.73	94.89	95.19
ω (g cm ⁻³)	R_j	2.83	1.01	9.37	11.95	6.45	8.68	4.69
	K_{1j}	5.71	5.98	6.08	5.91	6.28	5.93	6.10
	K_{2j}	6.26	6.20	6.11	6.31	6.10	6.17	6.11
	K_{3j}	6.39	6.18	6.17	6.14	5.98	6.26	6.15
	\bar{K}_{1j}	0.95	1.00	1.01	0.99	1.05	0.99	1.02
	\bar{K}_{2j}	1.04	1.03	1.02	1.05	1.02	1.03	1.02
A	R_j	0.68	0.22	0.09	0.40	0.30	0.33	0.05
	K_{1j}	114.88	103.79	119.32	107.96	112.17	121.33	109.35
	K_{2j}	112.76	114.10	120.11	115.97	118.13	117.45	118.28
	K_{3j}	115.57	125.32	103.78	119.28	112.91	104.43	115.58
	\bar{K}_{1j}	19.15	17.30	19.89	17.99	18.70	20.22	18.23
	\bar{K}_{2j}	18.79	19.02	20.02	19.33	19.67	19.58	19.71
	\bar{K}_{3j}	19.26	20.89	17.30	19.88	18.82	17.41	19.26
	R_j	2.81	21.53	16.33	11.32	5.96	16.90	8.93

As the NaHCO₃ dosage increased, the porosity of the CSF-PVFM first increased and then decreased, showing a normal distribution. As a foaming agent, NaHCO₃ reacted with sulfuric acid during the reaction process and quickly released carbon dioxide gas, forming a large number of bubbles in the composite material. A small NaHCO₃ dosage created too few carbon dioxide bubbles, leading to uneven pore formation. With the increase in NaHCO₃ dosage, the porosity gradually increased. When the NaHCO₃ dosage was 0.63 g, the porosity reached its maximum value. Later, the large dosage of NaHCO₃ reacted quickly with sulfuric acid, and the bubbles expanded rapidly in the material. The pores varied in size, which caused bubbles to easily burst.

The change in reaction temperature affected the progress of the acetal reaction. The porosity decreased with an increase in the reaction temperature. A high temperature is a disadvantage for acetal reaction. At a reaction temperature of 40°C, the polymerization was slow and the cell size was uniform. As the temperature increased to 50°C, the rate of the dissociation reaction of acetalization was considerably accelerated, which affected the acetal reaction process, and the bubbles generated gradually

expanded and ruptured, resulting in serious tearing of the pores of the material.

Based on the above experimental results, the appropriate combination level for the porosity of CSF-PVFM is $A_2B_3C_1D_2E_2F_1$ —that is, a PVA mass concentration of 10%, a CSF dosage of 0.5 g, a H₂SO₄ dosage of 4 mL, a HCHO dosage of 5 mL, a NaHCO₃ dosage of 0.63 g, and a reaction temperature of 40°C.

3.5.4. Analysis of the specific gravity

Fig. 6 and Table 9 depict the influences of various factors on the specific gravity of the CSF-PVFM, which follow the order PVA mass concentration > HCHO dosage > reaction temperature > NaHCO₃ dosage > CSF dosage > H₂SO₄ dosage. In this study, the PVA mass concentration and HCHO dosage were found to exercise the greatest influence, whereas the influence exercised by the remaining factors was less significant.

The specific gravity gradually increased with the increase in the PVA mass concentration. At a PVA mass concentration of 10%, the specific gravity of CSF-PVFM was close to that of water, so the biocarrier material CSF-PVFM

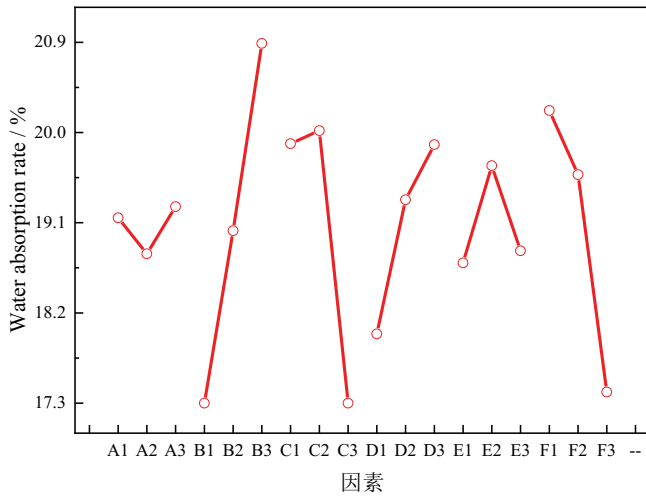


Fig. 7. Tend chart on water absorption.

could exhibit fluidization in water. However, when the PVA mass concentration exceeded 10%, the viscosity of the solution was too large, limiting the growth of bubbles with a certain amount of resistance. The obtained carrier material had a relatively compact structure, resulting in a low porosity and a large specific gravity for the material. Therefore, the optimal PVA mass concentration is 10%.

As the HCHO dosage increased, the specific gravity of the CSF-PVFM first increased and then decreased. When the amount of HCHO was too small, the degree of cross-linking was not enough. The amount of HCHO gradually increased, the degree of cross-linking continued to increase, so the specific gravity gradually also increased. When the amount of HCHO was 4 mL, the specific gravity reached the maximum and was close to 1. After that, the degree of cross-linking of CSF-PVFM increased with the increase in HCHO dosage, resulting in a high porosity between long molecular chains and then a decrease in the specific gravity.

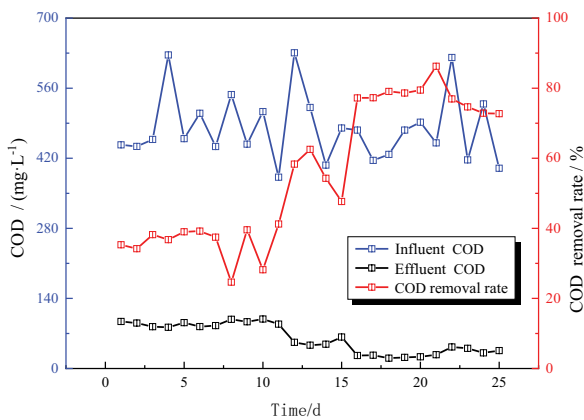
Based on the above experimental results, the appropriate combination level for the specific gravity of CSF-PVFM is $A_2B_1C_1D_1E_3F_1$ —that is, a PVA mass concentration of 10%, a CSF dosage of 0.4 g, a H_2SO_4 dosage of 4 mL, a HCHO dosage of 4 mL, a $NaHCO_3$ dosage of 0.68 g, and a reaction temperature of 40°C.

3.5.5. Analysis of the water absorption

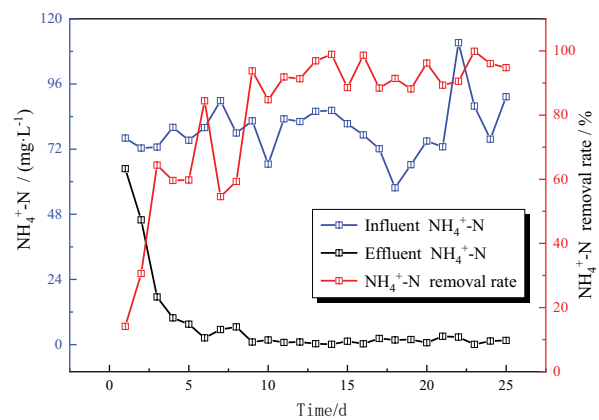
Fig. 7 and Table 10 depict the influences of various factors on the water absorption of the CSF-PVFM, which follow the order CSF dosage > reaction temperature > H_2SO_4 dosage > HCHO dosage > $NaHCO_3$ dosage > PVA mass concentration. In this orthogonal experiment, the former three were found to exercise the greatest influence, whereas the influence of the remaining factors was less significant.

With the increase in CSF dosage, the water absorption of CSF-PVFM showed an increasing trend. This occurred because the repeating units of macromolecules on the surface of straw fibers contain three hydroxyl groups in each base ring. These hydroxyl groups formed intramolecular or intermolecular hydrogen bonds, making the fibers exhibit strong polarity and hydrophilicity. CSF was added to the raw materials to introduce hydrophilic groups. As a result, the water absorption of CSF-PVFM increased, reaching maximum at 0.5 g. Therefore, 0.5 g was selected as the appropriate CSF dosage.

With the increase in the amount of the H_2SO_4 dosage, water absorption gradually increased, and at 4 mL water absorption reached maximum. Afterwards, water absorption decreased sharply with an increase in the amount of sulfuric acid. The reason was that the solidification of the foam and the gasification process of the blowing agent were carried out at the same time, and the speeds of these two processes must be balanced. When the amount of sulfuric acid was too large, the acetalization reaction was violent, and the end point of the reaction was difficult to control, a gel easily formed in the reaction kettle, resulting in a decrease in water absorption.



(a)



(b)

Fig. 8. Start-up period: removal efficiency of COD (a) and removal efficiency of NH_4^+-N (b).

Table 8
Analysis of variance on porosity

Source	SS	df	MS	F	Significance
A ^Δ	0.698	2	0.349		
B ^Δ	0.104	2	0.052		
C	7.942	2	3.971	8.80	2
D	15.605	2	7.803	17.30	1
E	3.770	2	1.885	4.18	4
F	6.430	2	3.215	7.13	3
e	1.901	2	0.951		
e ^Δ	2.703	6	0.451		

Table 9
Analysis of variance on specific gravity

Source	SS	df	MS	F	Significance
A ^Δ	0.0468	2	0.0234	26.00	1
B ^Δ	0.0036	2	0.0018		
C	0.0012	2	0.0006		
D ^Δ	0.0108	2	0.0054	6.00	2
E ^Δ	0.0078	2	0.0039	4.33	4
F ^Δ	0.0084	2	0.0042	4.67	3
e	0.0006	2	0.0003		
e ^Δ	0.0054	6	0.0009		

Water absorption reached its maximum at 40°C and then decreased as the temperature increased. When the reaction temperature was lower, the reaction was slower. The speed of bubble generation and the speed of curing were almost balanced, and the generated bubbles gradually expanded and solidified, which gave the CSF-PVFM a better pore structure and high water absorption. However, as the temperature rose, the reaction rate of the acetal reaction was accelerated, making it difficult to control the end point of the experiment, causing a lot of foam to burst, leaving few pores, a hard texture, and low water absorption.

Based on the above experimental results, the appropriate combination level for water absorption of CSF-PVFM is $A_3B_3C_2D_3E_2F_1$ —that is, a PVA mass concentration of 11%, a CSF dosage of 0.5 g, a H_2SO_4 dosage of 4 mL, a HCHO dosage of 5 mL, a $NaHCO_3$ dosage of 0.63 g, and a reaction temperature of 40°C.

Multiple comparisons were made among different levels of each influencing factor with differing significance.

When the porous material acts as a suspension material, porosity and specific gravity have greater impacts on the material, followed by water absorption. According to this, for factor A, the optimal levels of porosity, specific gravity and water absorption are A_2 , A_1 and A_2 , respectively. It could be seen that the second level had the greatest impact on the experiment, so A_2 was the optimal level. Finally, the best combination of factors was $A_2B_3C_2D_2E_2F_1$. Therefore, the optimal preparation condition of CSF-PVFM was as follows: a PVA mass concentration of 10%, a CSF dosage of 0.5 g, a H_2SO_4 dosage of 4 mL, a HCHO dosage of 5 mL,

Table 10
Analysis of variance on water absorbency rate

Source	SS	df	MS	F	Significance
A	0.725	2	0.363		
B	38.687	2	19.344	10.56	1
C ^Δ	28.247	2	14.124	7.71	2
D	11.341	2	5.671	3.10	4
E ^Δ	3.356	2	1.678		
F	26.029	2	13.015	7.10	3
e	6.908	2	3.454		
e ^Δ	10.989	6	1.832		

a SDS dosage of 0.3 g, a $NaCO_3$ dosage of 0.63 g, and a reaction temperature of 40°C. The dripping time of the sulfuric acid was 6 min and of the formaldehyde was 4 min. The curing time was 8 h at 60°C.

Finally, the experiment was repeated under optimal synthesis conditions to confirm that they truly optimized the performance. Table 11 shows that the average porosity of CSF-PVFM can reach 97.2%, the specific gravity can average 1 g cm^{-3} , the water absorption can reach 22.58, and the degree of cross-linking 96.08%. All of these figures are higher than those of any previous orthogonal experimental result, so the properties of the material have been maximally improved under the optimal synthesis conditions.

3.6. Analysis of the sewage treatment effect

The effect of CSF-PVFM sewage treatment was researched in this experiment by examining the removal rate of COD and ammonia nitrogen.

3.6.1. The start-up period

The start-up period mainly involved the cultivation of biofilm on the CSF-PVFM suspended biocarrier. The microorganisms mainly came from sewage that contained fewer microorganisms, so the hanging time was longer. After the system ran continuously for 30 d, the COD removal rate exceeded 70%, and the ammonia nitrogen removal rate exceeded 90% in Fig. 8. It is believed that the biofilm was successfully cultured and had entered the rising period. At this time, the volume load was stable at 0.2 kg ($m^{-3} d^{-1}$), and the starting state was basically stable.

3.6.2. The elevated period

The elevated period of the system lasted 60 d, and the volume load increased from 0.2 to 0.4 kg ($m^{-3} d^{-1}$). When the system volume load was 0.2 kg ($m^{-3} d^{-1}$), the average removal rate of COD was 85.55% and the average removal rate of ammonia nitrogen was 95.75%, presented in Fig. 9. When the system volume load was 0.3 kg ($m^{-3} d^{-1}$), the average removal rate of COD was 89.44% and the average ammonia nitrogen removal rate was 96.7%, presented in Fig. 10. When the system volume load was 0.4 kg ($m^{-3} d^{-1}$), the average COD removal rate was 93.24% and the average ammonia nitrogen removal rate was 96.61%, presented

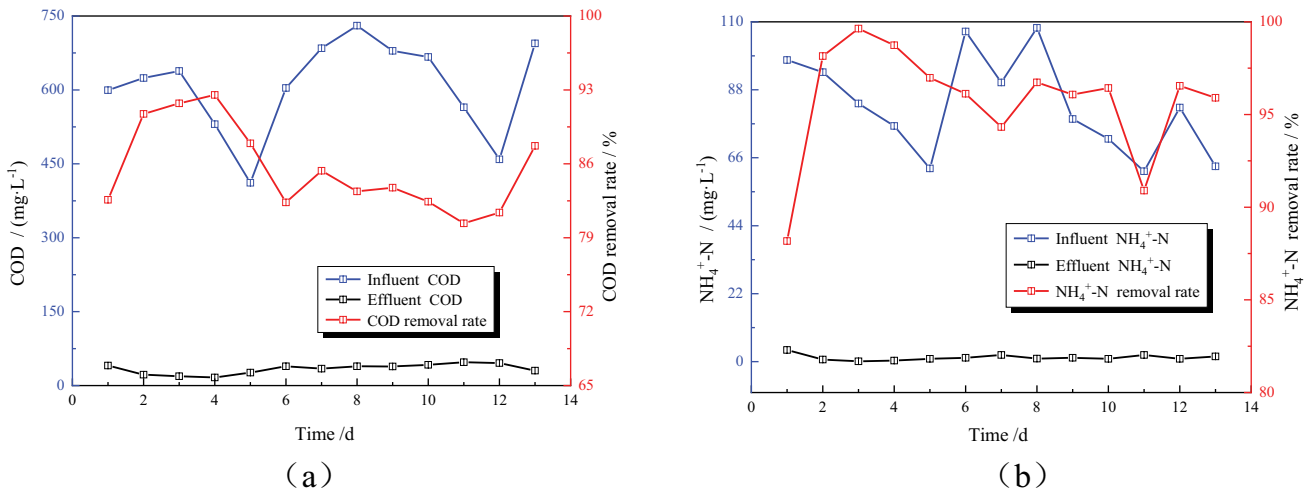


Fig. 9. Volume load was 0.2 kg (m⁻³ d⁻¹): removal efficiency of COD (a) and removal efficiency of NH₄⁺-N (b).

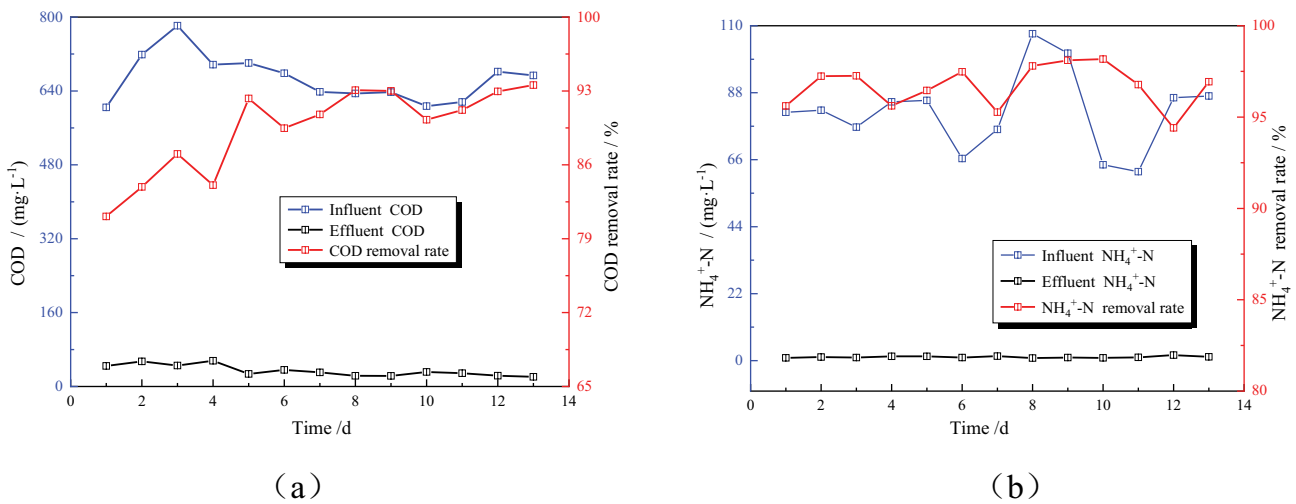


Fig. 10. Volume load was 0.3 kg (m⁻³ d⁻¹): removal efficiency of COD (a) and removal efficiency of NH₄⁺-N (b).

in Fig. 11. The above results indicated that the system would enter a stable period.

3.6.3. The stable period

The system volume load was maintained at 0.4 kg (m⁻³ d⁻¹). After 30 d of continuous operation, the average COD removal rate of CSF-PVFM reached 92.84% and the average removal rate of ammonia nitrogen reached 96.66%, presented in Fig. 12. This showed that CSF-PVFM had good removal ability and stable removal effect on COD after being attached to biofilm and that it had a strong impact load resistance. At the same time, the removal effect of ammonia nitrogen was relatively good. This was because the outer layer of the CSF-PVFM was an aerobic zone for nitrification, while the inside was an anoxic and anaerobic zone for denitrification to achieve the overall denitrogenation effect of the system. In addition, because the microorganisms

attached to the CSF-PVFM had a higher sludge age, the nitrifying bacteria and submarketing bacteria with a long generation time could grow and multiply, which enhanced the sewage denitrification effect. Finally the effluent COD was less than that of 50 mg L⁻¹, and the effluent ammonia nitrogen was less than that of 5 mg L⁻¹, which reached the first-level discharge standard of the national standard, the “Emission Standard of Pollutants for Urban Sewage Treatment Plants”. Therefore, CSF-PVFM has a good removal rate of COD and ammonia nitrogen from sewage.

In recent years, several studies have been conducted to evaluate the efficiency of different carriers in MBBR for sewage treatment (Table 12). Hence, it is evident that different types of biocarriers play a crucial role in affecting the pollutant removal efficiency of MBBR. Moreover, there are few studies on the application of PVFM as a biological carrier to MBBR, and the pollutant removal effect of most carriers is not as good as that of CSF-PVFM.

Table 11
Repeat experiments

Treatment	Porosity (%)	Specific gravity (g cm ⁻³)	Water absorption	Cross-linking degree (%)
1	97.23	0.99	22.79	95.98
2	96.87	1.01	23.07	95.88
3	97.50	0.99	21.88	96.37
Mean	97.20	1.00	22.58	96.08

Table 12
The pollutant removal efficiency of various carriers in MBBR set-up

Biocarrier/Support material	Pollutant removal effects	
	Removal rate of COD	Removal rate of ammonia nitrogen
PVA (Polyvinyl alcohol) gel [35]	90%	91.7%
Polyurethane foam (PUF) [36]	81%	95.6%
Polyester-polyurethane sponge with plastic carrier [37]	93.16% ± 1.45%	81.30% ± 2.03%
Polyethylene (HDPE) [38]	87.89%	87.98%
Novel surface-modified polyethylene (PE) carriers [39]	90.5%	88.6%
Conventional polyethylene (PE) carriers [39]	89.7%	82.3%

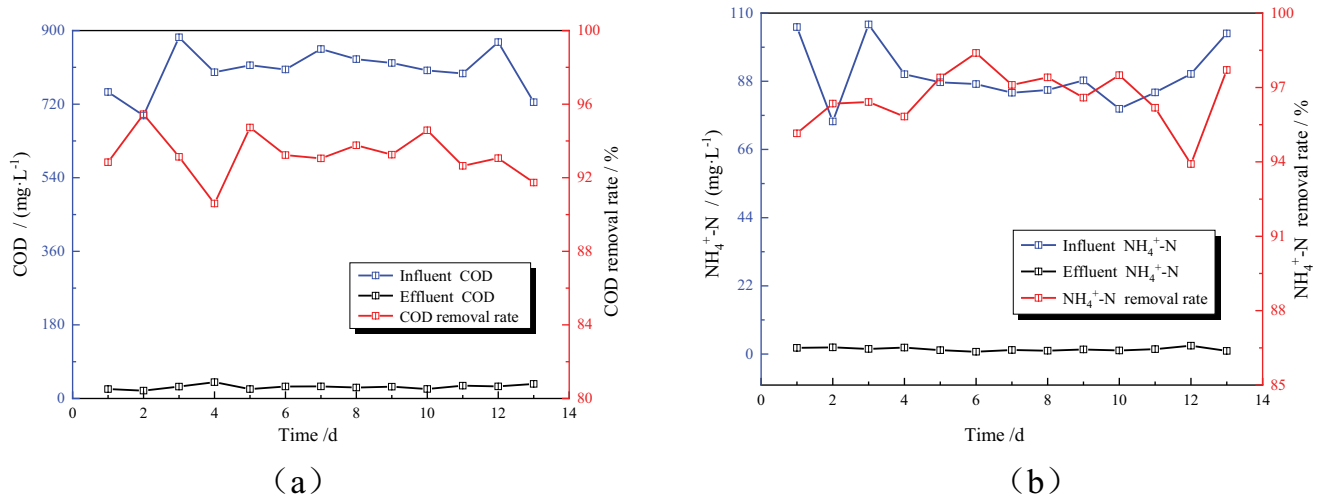


Fig. 11. Volume load was 0.4 kg (m⁻³ d⁻¹): removal efficiency of COD (a) and removal efficiency of NH₄⁺-N (b).

4. Conclusions

- The suspended biocarrier CSF-PVFM was successfully prepared in this study. The results of FTIR and XRD indicate that CSF could possibly have cross-links with PVA through the (–OH) hydroxyl group. The biocarrier material has a good three-dimensional network structure, wide pore size range, and high surface area, according to the SEM and BET analyses. Additionally, according to tensile strength and TGA analysis results, the mechanical properties and thermal stability of the material improved.
- The raw material ratios and preparation technology conditions were optimized through the single-factor

experiment and the orthogonal experiment. The main conclusions were as follows: (1) through the orthogonal test, a biocarrier material could be obtained, with good porosity, water absorption, and a specific gravity close to that of water; (2) the orthogonal test method was used to study the influence of the PVA mass concentration (A), CSF dosage (B), H₂SO₄ dosage (C), HCHO dosage (D), NaHCO₃ dosage (E), and reaction temperature (F) on the performance of the CSF-PVFM. The order of the influence of each factor on the porosity by significance was D > C > F > E > A > B. The order of the influence of each factor on the specific gravity of the solidified material by significance was A > D > F > E > B > C. The order of the influence of each factor on the water

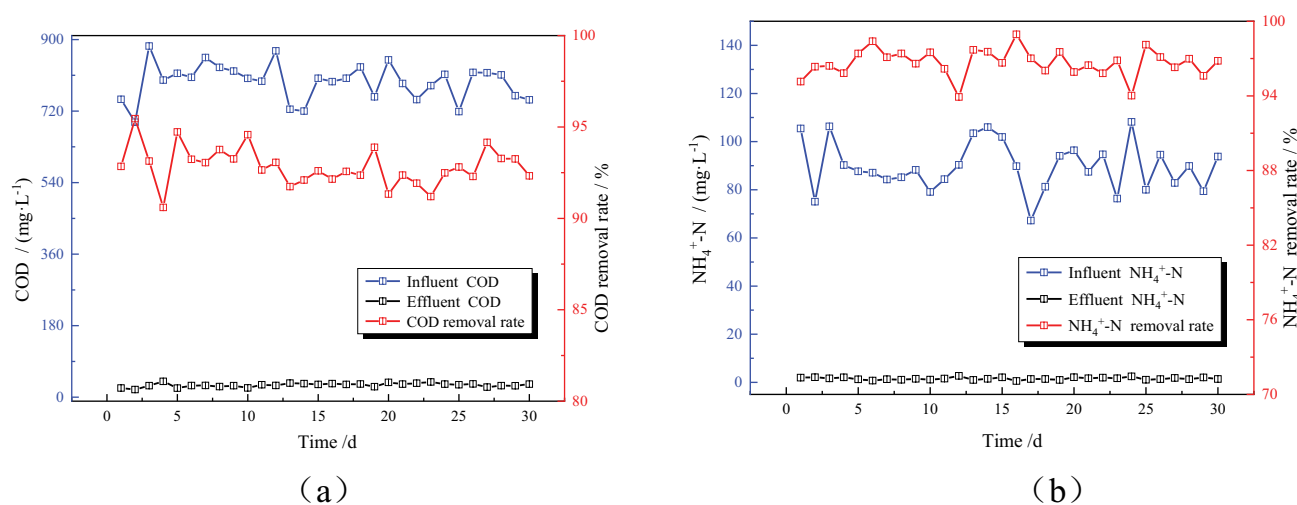


Fig. 12. Stable period: removal efficiency of COD (a) and removal efficiency of NH₄⁺-N (b).

absorption by significance was $B > F > C > D > E > A$; and (3) through the one-by-one analysis of different levels under the same factor, the optimal raw material ratio and preparation technology conditions were obtained, namely a PVA mass concentration of 10%, a CSF dosage of 0.5 g, a H₂SO₄ dosage of 4 mL, a HCHO dosage of 5 mL, a SDS dosage of 0.3 g, a Na₂CO₃ dosage of 0.63 g, and a reaction temperature of 40°C.

- In addition, as a suspended biocarrier, the CSF-PVFM was used for sewage treatment, which was prepared under optimal experimental conditions. After the system was stabilized, the average removal rates of COD and ammonia nitrogen were 92.84% and 96.66%, respectively. By comparing the experimental results of sewage treatment with related literature, it has been confirmed that the CSF-PVFM suspended biocarrier has an excellent pollutant removal performance in sewage treatment.
- In short, the CSF-PVFM suspended biocarrier has the advantages of high-performance, better manufacturability, low cost, and little pollution. The proposed CSF-PVFM biocarrier can thus be recommended as a green and economically feasible novel suspended biocarrier in sewage treatment. However, it is recommended to further study the regeneration performance of the biocarrier in the future in order to improve the utilization rate and to save on the costs.

Symbols

ε	—	Porosity, %
m	—	Mass of dry material, g
ρ	—	Density of dry material, g cm ⁻³
ω	—	Specific gravity, g cm ⁻³
V	—	Volume of dry material, cm ³
M	—	Mass of the material immersed in distilled water and fully expanded, g
A	—	Water absorption
J	—	Cross-linking degree, %
m_1	—	Mass of material, g

m_2 — Mass of the material after putting it in distilled water at 95°C for 24 h, g

References

- [1] S.A. Ismail, W.L. Ang, A.W. Mohammad, Electro-Fenton technology for wastewater treatment: a bibliometric analysis of current research trends, future perspectives and energy consumption analysis, *J. Water Process Eng.*, 40 (2021) 101952, doi: 10.1016/j.jwpe.2021.101952.
- [2] D. Han, M.J. Currell, G. Cao, Deep challenges for China's war on water pollution, *Environ. Pollut.*, 218 (2016) 1222–1233.
- [3] C.E. Santo, V.J. Vilar, A. Bhatnagar, E. Kumar, C.M. Botelho, R.A. Boaventura, Biological treatment by activated sludge of petroleum refinery wastewaters, *Desal. Water Treat.*, 51 (2013) 6641–6654.
- [4] L.L. Albornoz, L. Marder, T. Benvenuti, A.M. Bernardes, Electrodialysis applied to the treatment of an university sewage for water recovery, *J. Environ. Chem. Eng.*, 7 (2019) 102982, doi: 10.1016/j.jece.2019.102982.
- [5] M. Mousazadeh, S.M. Alizadeh, Z. Frontistis, I. Kabdaşlı, E.K. Niaragh, Z. Al Qodah, Z. Naghdali, A. El Din Mahmoud, M.A. Sandoval, E. Butler, M.M. Emamjomeh, Electrocoagulation as a promising defluoridation technology from water: a review of state of the art of removal mechanisms and performance trends, *Water*, 13 (2021) 656, doi: 10.3390/w13050656.
- [6] M. Rezakazemi, A. Khajeh, M. Mesbah, Membrane filtration of wastewater from gas and oil production, *Environ. Chem. Lett.*, 16 (2018) 367–388.
- [7] Z. Huang, Y. Li, W. Chen, J. Shi, N. Zhang, X. Wang, Z. Li, L. Gao, Y. Zhang, Modified bentonite adsorption of organic pollutants of dye wastewater, *Mater. Chem. Phys.*, 202 (2017) 266–276.
- [8] M. Ksibi, Chemical oxidation with hydrogen peroxide for domestic wastewater treatment, *Chem. Eng. J.*, 119 (2006) 161–165.
- [9] Y. Jiang, H. Zhao, J. Liang, L. Yue, T. Li, Y. Luo, Q. Liu, S. Lu, A.M. Asiri, Z. Gong, X. Sun, Anodic oxidation for the degradation of organic pollutants: Anode materials, operating conditions and mechanisms. A mini review, *Electrochem. Commun.*, 123 (2021) 106912, doi: 10.1016/j.elecom.2020.106912.
- [10] M. Mousazadeh, Z. Naghdali, Z. Al-Qodah, S.M. Alizadeh, E. Karamati Niaragh, S. Malekmohammadi, P.V. Nidheesh, E.P.L. Roberts, M. Sillanpää, M.M. Emamjomeh, A systematic diagnosis of state of the art in the use of electrocoagulation as a sustainable technology for pollutant treatment: an updated

- review, *Sustainable Energy Technol. Assess.*, 47 (2021) 101353, doi: 10.1016/j.seta.2021.101353.
- [11] C. Tao, T. Peng, C. Feng, N. Chen, Q. Hu, C. Hao, The feasibility of an up-flow partially aerated biological filter (U-PABF) for nitrogen and COD removal from domestic wastewater, *Bioresour. Technol.*, 218 (2016) 307–317.
- [12] R. Su, G. Zhang, P. Wang, S. Li, R.M. Ravenelle, J.C. Crittenden, Treatment of antibiotic pharmaceutical wastewater using a rotating biological contactor, *J. Chem.*, 2015 (2015) 705275, doi: 10.1155/2015/705275.
- [13] M. Lu, X. Wei, Y. Su, Aerobic treatment of oilfield wastewater with a bio-contact oxidation reactor, *Desal. Water Treat.*, 27 (2011) 334–340.
- [14] A.D. Santos, R.C. Martins, R.M. Quinta-Ferreira, L.M. Castro, Moving bed biofilm reactor (MBBR) for dairy wastewater treatment, *Energy Rep.*, 6 (2020) 340–344.
- [15] L. Chu, J. Wang, Comparison of polyurethane foam and biodegradable polymer as carriers in moving bed biofilm reactor for treating wastewater with a low C/N ratio, *Chemosphere*, 83 (2011) 63–68.
- [16] X. Guo, B. Li, R. Zhao, J. Zhang, L. Lin, G. Zhang, R.-H. Li, J. Liu, P. Li, Y. Li, X.-Y. Li, Performance and bacterial community of moving bed biofilm reactors with various biocarriers treating primary wastewater effluent with a low organic strength and low C/N ratio, *Bioresour. Technol.*, 287 (2019) 121424, doi: 10.1016/j.biortech.2019.121424.
- [17] K. Haribabu, V. Sivasubramanian, Biodegradation of organic content in wastewater in fluidized bed bioreactor using low-density biosupport, *Desal. Water Treat.*, 57 (2016) 4322–4327.
- [18] Y.H. Liu, X.Z. Lu, M. Zhao, X. Hu, X.M. Sun, Preparation of new filler pvf and its performance of simultaneous nitrification and denitrification, *Technol. Water Treat.*, 32 (2006) 36–40 (in Chinese).
- [19] S.W. Wu, G.C. Li, N. Li, Preparation of novel polyvinyl formal composites, *Adv. Fine Petrochem.*, 10 (2009) 38–41 (in Chinese).
- [20] Y. Zhang, Z.S. Ya'e Wang, J. Li, Y. Mao, Preparation and property of PVFM/attapulgit carrier for microorganism immobilization, *Polym. Mater. Sci. Eng. (Chengdu, China)*, 28 (2012) 140–143 (in Chinese).
- [21] S.J. Feng, L. Xu, L.F. Wang, H.G. Liu, T.L. Luo, G.J. Liu, Study on preparation and properties of activated carbon/fly ash-PVFM composite materials, *China Plast. Ind.*, 41 (2013) 117–120 (in Chinese).
- [22] C. Hernandez, F. Ferreira, D. Rosa, X-ray powder diffraction and other analyses of cellulose nanocrystals obtained from corn straw by chemical treatments, *Carbohydr. Polym.*, 193 (2018) 39–44.
- [23] S. Wang, X. Guo, T. Liang, Y. Zhou, Z. Luo, Mechanism research on cellulose pyrolysis by Py-GC/MS and subsequent density functional theory studies, *Bioresour. Technol.*, 104 (2012) 722–728.
- [24] M. Gupta, T.B. Rawal, P. Dupree, J.C. Smith, L. Petridis, Spontaneous rearrangement of acetylated xylan on hydrophilic cellulose surfaces, *Cellulose*, 28 (2021) 3327–3345.
- [25] S.J. Feng, Study on the Preparation and Application on Sewage Treatment of the Suspended Carrier PVFM Compositd with Natural Fiber, Master's Thesis, Zhengzhou University, Zhengzhou, China, 2013. Available at: <https://kns.cnki.net/KCMS/detail/detail.aspx?dbname=CMFD201302&filename=1013255384.nh/> (in Chinese).
- [26] D.R. Lima, L. Klein, G.L. Dotto, Application of ultrasound modified corn straw as adsorbent for malachite green removal from synthetic and real effluents, *Environ. Sci. Pollut. Res.*, 24 (2017) 21484–21495.
- [27] C. Salom, M. Prolongo, A. Toribio, A. Martínez-Martínez, I.A. de Cárcer, S. Prolongo, Mechanical properties and adhesive behavior of epoxy-graphene nanocomposites, *Int. J. Adhes. Adhes.*, 84 (2018) 119–125.
- [28] A. Moslemi, B.N. Neya, M.R. Davoodi, M. Dehestani, Numerical investigation of post-tensioned concrete slab developed by hybrid concrete, PU foams, PVC, and GFRP, *Int. J. Adv. Eng. Sci. Appl. Math.*, 13 (2021) 344–359.
- [29] M.W. Mirza, T.C. D'Silva, K.M. Gani, S.S. Afsar, R.Z. Gaur, P.K. Mutiyar, A.A. Khan, V. Diamantis, B. Lew, Cultivation of anaerobic ammonium oxidizing bacteria (AnAOB) using different sewage sludge inoculums: process performance and microbial community analysis, *J. Chem. Technol. Biotechnol.*, 96 (2021) 454–464.
- [30] Y. Cao, C. Zhang, H. Rong, G. Zheng, L. Zhao, The effect of dissolved oxygen concentration (DO) on oxygen diffusion and bacterial community structure in moving bed sequencing batch reactor (MBSBR), *Water Res.*, 108 (2017) 86–94.
- [31] A. Pourjavadi, Z. Mazaheri Tehrani, H. Salami, F. Seidi, A. Motamedi, A. Amanzadi, E. Zayerzadeh, M. Shabanian, Both tough and soft double network hydrogel nanocomposite based on o-carboxymethyl chitosan/poly(vinyl alcohol) and graphene oxide: a promising alternative for tissue engineering, *Polym. Eng. Sci.*, 60 (2020) 889–899.
- [32] Y. Zhang, H. Mu, H. Gao, H. Chen, W. Wu, Y. Han, X. Fang, C. Tong, Preparation of modified polyvinyl formal vibration-damping material and its application in strawberry, *J. Food Biochem.*, 45 (2021) e13647, doi: 10.1111/jfbc.13647.
- [33] Q. Li, P. Yu, T. Zhu, L. Zhang, Q. Li, Y. Luo, Pervaporation performance of crosslinked PVA and chitosan membranes for dehydration of caprolactam solution, *Desal. Water Treat.*, 16 (2010) 304–312.
- [34] F. Morgan-Sagastume, Biofilm development, activity and the modification of carrier material surface properties in moving-bed biofilm reactors (MBBRs) for wastewater treatment, *Crit. Rev. Env. Sci. Technol.*, 48 (2018) 439–470.
- [35] S.A. Osmani, A. Rajpal, A. Kazmi, Upgradation of conventional MBBR into aerobic/anoxic/aerobic configuration: a case study of carbon and nitrogen removal based sewage treatment plant, *J. Water Process Eng.*, 40 (2021) 101921, doi: 10.1016/j.jwpe.2021.101921.
- [36] Q. Feng, Y. Wang, T. Wang, H. Zheng, L. Chu, C. Zhang, H. Chen, X. Kong, X.-H. Xing, Effects of packing rates of cubic-shaped polyurethane foam carriers on the microbial community and the removal of organics and nitrogen in moving bed biofilm reactors, *Bioresour. Technol.*, 117 (2012) 201–207.
- [37] L. Deng, W. Guo, H. Hao Ngo, X. Zhang, X.C. Wang, Q. Zhang, R. Chen, New functional biocarriers for enhancing the performance of a hybrid moving bed biofilm reactor–membrane bioreactor system, *Bioresour. Technol.*, 208 (2016) 87–93.
- [38] N. Alisa, Y.S. Purnomo, Penurunan Kandungan Polutan Pada Air Limbah Industri Tempe Menggunakan Moving Bed Biofilm Reactor (MBBR), *EnviroUS*, 1 (2020) 42–47.
- [39] T. Liu, G. Jia, J. Xu, X. He, X. Quan, Simultaneous nitrification and denitrification in continuous flow MBBR with novel surface-modified carriers, *Environ. Technol.*, 42 (2021) 3607–3617.